Actin-based motility of vaccinia virus

Sally Cudmore*, Pascale Cossart†, Gareth Griffiths* & Michael Way*‡

* Cell Biology Programme, European Molecular Biology Laboratory, 1 Meyerhofstrasse, Heidelberg 69117, Germany
† Unité des Interactions Bacteries Cellules, Institut Pasteur, 25 rue du Dr Roux, 75724 Paris Cedex 15, France
‡ To whom correspondence should be addressed

THE role of the cytoskeleton during viral infection is poorly understood. Here we show, using a combination of mutant and drug studies, that the intracellular enveloped form of vaccinia virus is capable of inducing the formation of actin tails that are strikingly similar to those seen in *Listeria*, *Shigella* and *Rickettsia* infections. Analysis using video microscopy reveals that single viral particles are propelled *in vivo* on the tip of actin tails, at a speed of 2.8 μm min^{-1}. On contact with the cell surface, virus particles extend outwards on actin projections at a similar rate, to contact and infect neighbouring cells. Given the similarities between the motility of vaccinia virus and bacterial pathogens, we suggest that intracellular pathogens have developed a common mechanism to exploit the actin cytoskeleton as a means to facilitate their direct spread between cells.

Vaccinia virus, a close relative of the smallpox virus, has a genome of ~190 kilobase pairs (kbp) encoding over 260 potential open reading frames (ORFs), and so is one of the largest and most complex viruses known[1,2]. It is different from other viral families in that it has two distinct infectious forms, the intracellular mature virus (IMV) and the extracellular enveloped virus (EEV). IMV begin to appear about 4 hours post-infection, and are only released when the cell lyses, presumably as a result of the cytotoxic effects of infection. Alternatively, a small proportion of IMV can become wrapped by membrane cisternae derived from the *trans* Golgi network to form the intracellular enveloped virus (IEV), which is first seen about 6 hours post-infection[3,4]. Infectious EEV are thought to be released when the outermost membrane of the IEV fuses with the plasma membrane[3,5].

High-voltage electron microscopy has previously shown that, late in infection, vaccinia induces the formation of large microvilli with single virus particles at their tip[6]. Subsequent studies confirmed that actin was present in these microvilli[7–10]. We found in all cell types tested that ~6 hours post-infection the vaccinia virus strain WR begins to induce the formation of actin-containing structures that are very reminiscent of the actin tails formed during bacterial infection[11–15] (Fig. 1). Infection also results in a significant decrease in the number of actin stress fibres in the cell. Actin tail formation occurs from single viral particles, which always remain at the tip of these structures (Fig. 1*b*). Actin tails are initially seen in the interior of the cell, but as infection proceeds increasing numbers are seen projecting from the cell surface (Fig. 1*c*). Intracellular actin tails, which taper away from the virus, are typically 6.4–9.6 μm long ($n = 64$), whereas projections can reach lengths of over 20 μm. Electron microscopy confirms that single viral particles are in direct contact with actin filaments (Fig. 1*d*), which is consistent with the overlap between actin and virus particles seen in fluorescence images (Fig. 1*c*).

Although actin is necessary in the later stages of infection, it is not essential during the initial stages of infection or IMV assembly, as these processes occur in cells infected in the presence of cytochalasin D (data not shown). However, the presence of cytochalasin D prevents the formation of tails and subsequent release of IEV, although actin tails are able to form rapidly when cytochalasin D is removed (data not shown).

The time of appearance and number of viral particles inducing actin tails (5–15%) is consistent with the formation of IEV during vaccinia virus infection of HeLa cells[3]. We tested whether IEV, and not IMV, induces the formation of actin tails using both the vaccinia mutant, vRB 12, which is highly deficient in the production of IEV[16] and the drug N_1-isonicotinoyl-N_2-3-methyl-4-chlorobenzoylhydrazine (IMCBH), which blocks IEV formation[16–20]. In both cases, IMV is confined to the perinuclear

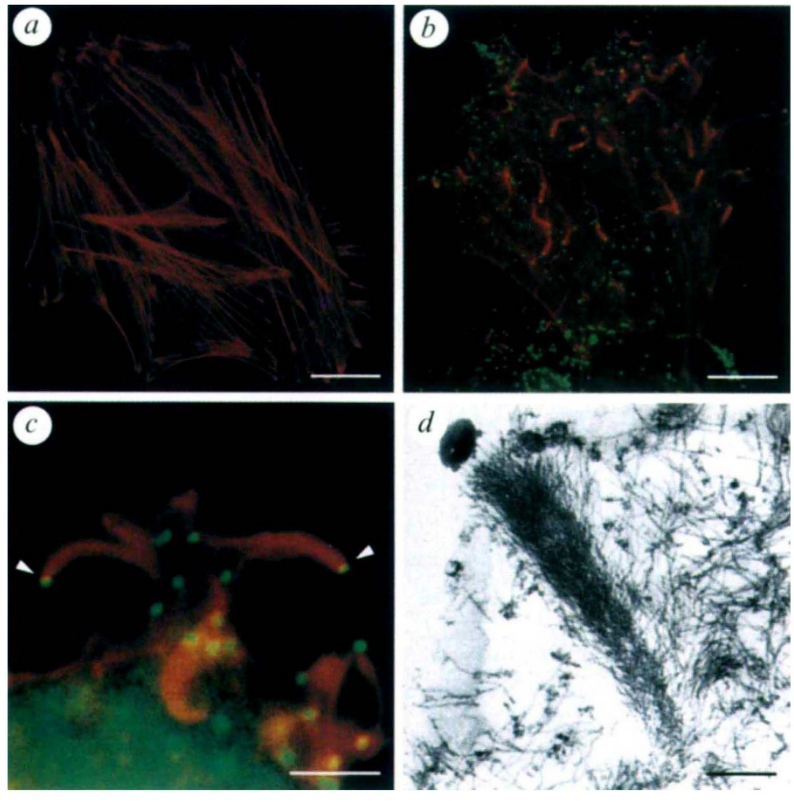

FIG. 1 Actin tails in HeLa cells infected with vaccinia virus. *a*, Uninfected control HeLa cell which shows a typical actin stress fibre staining. Scale bar, 50 μm. *b*, Infected cells showing intracellular actin tails (red) and viral particles (green). Scale bar, 50 μm. *c*, Viral particles projecting from the cell surface on actin tails show a clear overlap between the viral particle and actin (white arrowheads). Scale bar, 10 μm. *d*, Electron micrograph of an actin tail decorated with S1 myosin showing a direct contact between actin filaments and the virus particle. Scale bar, 400 nm.

METHODS. *a–c*, HeLa cells were infected with vaccinia virus strain WR at a multiplicity of infection of one plaque-forming unit per cell. The cells were fixed 8 h after infection and stained as described[29] with rhodamine phalloidin and the anti-vaccinia antibody, C3, which recognizes the peripheral membrane protein of relative molecular mass 14,000 (M_r 14K) of the IMV[30], followed by FITC goat anti-mouse. *d*, Infected HeLa cells were made permeable with 1 U ml^{-1} streptolysin O (SLO) in SLO buffer (150 mM sucrose, 50 mM KAc, 5 mM MgAc, 10 mM HEPES, 1 mM DTT) on ice for 10 min followed by a 15-min incubation at 37 °C. The cells were washed once in 50 mM phosphate buffer (pH 6.8) and incubated with 2 mg ml^{-1} S1 myosin for 30 min on ice. After two washes in ice-cold PBS, the cells were fixed in 1% gluteraldehyde and 2% tannic acid for 30 min. The specimens were then post-fixed in 1% osmium on ice for 30 min, dehydrated in ethanol, and embedded in EPON.

© 1995 Nature Publishing Group

region of the cell, and no actin tails are seen while the actin cytoskeleton appears normal (Fig. 2). Subsequent removal of IMCBH results in the appearance of actin tails with associated viral particles (Fig. 2*c*).

We observed individual viral particles *in vivo* by video microscopy (Fig. 3). Phase-dense structures, the actin tails, were only observed behind moving viral particles and were completely absent from vRB12-infected cells. The number of moving particles and tails is consistent with fluorescence images of fixed cells, although the tails generally appear shorter. Movement within cells appears to be random with an average speed of 2.8 μm min^{-1} (s.d. 0.5 μm min^{-1}, $n=44$), which is similar to that observed for *Listeria*[21,22]. On reaching the cell surface, virus particles project up to 20 μm at the same rate (Fig. 3). Projections are always much larger than the normal cell-surface microvilli, and presumably correspond to the virally induced projections previously described[6,7].

Cytochalasin D has previously been shown to prevent the release of IEV, which suggests that actin is involved in this process[23]. Our immunofluorescence images clearly show viral-tipped actin projections extending into uninfected cells (Fig. 4*a*). Electron microscopy also shows virus particles at the tip of a dense actin network projecting from one cell into another (Fig. 4*b*). Taken together, our results suggest that IEV are able to recruit and exploit actin to facilitate their spread from cell to cell. Given that the rates at which intracellular tails move and projections extend are identical, it is likely that these two events are driven by the same mechanism. However, the stability of actin in tails and projections is very different: the actin at the distal end of the intracellular tail is unstable and depolymerizes as the tail continues to extend, but it is stable in the elongating projection. This stability may be explained in part by membrane interactions in the projection that are absent in intracellular tails.

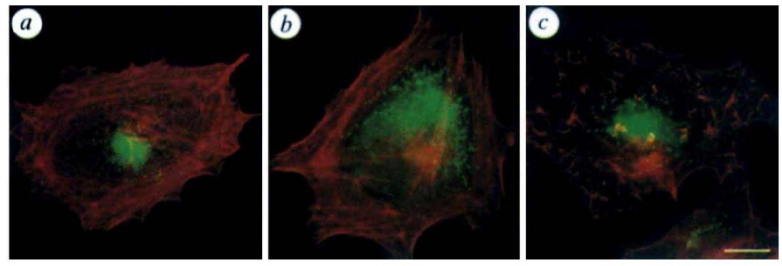

FIG. 2 IEV induces actin tail formation. *a*, HeLa cells infected with a mutant vaccinia strain, vRB 12. *b*, Cells infected with wild-type WR in the presence of IMCBH. The virus is concentrated in the perinuclear area of both cells and there are no actin tails. *c*, Viral particles are seen on actin tails 1 h after IMCBH removal. Scale bar, 50 μm.
METHODS. Cells were infected with WR or vRB12 as described above. IMCBH was added to a final concentration of 10 μg ml^{-1} 1 h post-infection. At 8 h post-infection cells were washed 5 times with PBS and fixed 1 h after washout.

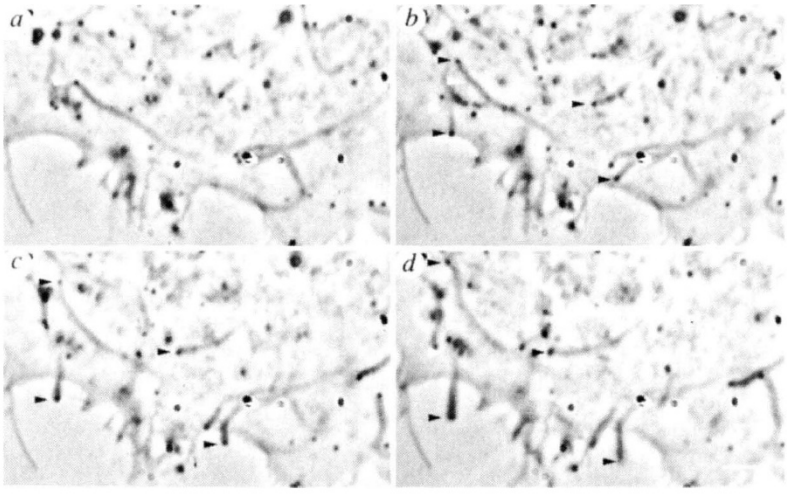

FIG. 3 Virus motility *in vivo*. Frame stills 40 s apart, from the video microscope, showing virus particles moving through the cell at the tip of actin tails and inducing the formation of protrusions from the cell surface. White arrowheads are fixed reference points, and black arrows indicate moving virus particles. Scale bar, 3.0 μm.
METHODS. Cells were infected with WR and viewed 10 h post-infection with a Zeiss axiovert microscope using a Sony CCD IRIS camera.

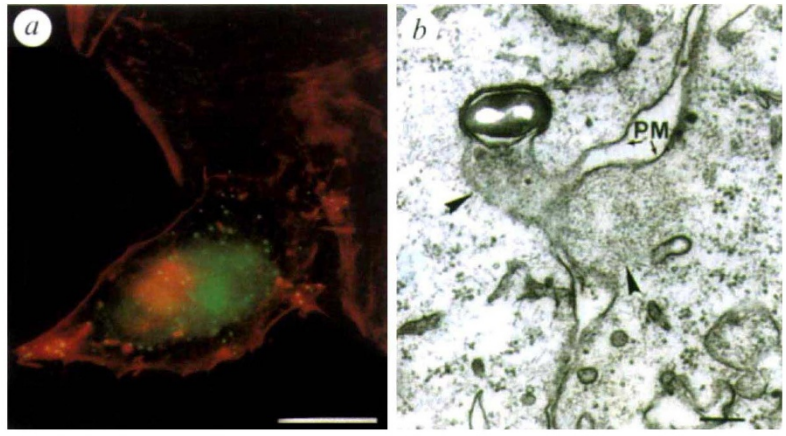

FIG. 4 Spread of vaccinia virus from cell to cell. *a*, Virus particles moving from an infected cell to an uninfected cell at the tip of actin-rich projections. Scale bar, 50 μm. *b*, Electron micrograph of a virus particle moving into a neighbouring cell. Black arrowheads show actin, and PM indicates the plasma membrane of the two cells. Scale bar, 400 nm.
METHODS. *a*, Cells were infected in the presence of IMCBH. Then, 5 h post-infection, the cells were washed once with warm PBS + IMCBH and uninfected cells were seeded on the same coverslips; 3 h later the IMCBH was washed out, and the cells were fixed after 1 h and stained as described above. *b*, Infected cells were fixed in 1% gluteraldehyde, 0.5 mg ml^{-1} saponin, 2% tannic acid, 50 mM KCl, 5 mM $MgCl_2$ for 30 min, post-fixed in 1% osmium on ice for 30 min, dehydrated in ethanol, and embedded in EPON.

© 1995 Nature Publishing Group

The intimate relationship between the IEV and the actin cytoskeleton suggests that the virus contains protein(s) that can associate directly or indirectly with actin. In *Listeria* species and *Shigella*, the proteins ActA, IactA and IcsA are critical for the nucleation of actin filaments at the bacterium surface[15,24,26]. Sequence comparisons of the vaccinia virus genome with ActA, IactA or IcsA failed to identify any ORF that contains significant homologous sequences. One possible candidate for viral interactions with actin is the A42R ORF, which is 32.1% identical to human profilin[27]. However, deletion of A42R has previously shown that it is not required for infectivity or release of mature virions[27]. Moreover, we found that vaccinia virus lacking A42R is still able to form actin tails and projections (data not shown), which is consistent with the recent observation that profilin is not required for actin-based motility of *Listeria* in the cell-free *Xenopus* system[28]. Whether profilin is involved in vaccinia motility will require further characterization, as the virus may be able to utilize cellular profilin isoforms. Given the similarities between the motility of bacterial pathogens and vaccinia virus, we suggest that intracellular pathogens have developed a common mechanism to exploit the actin cytoskeleton for their own purposes. □

Received 25 August; accepted 6 October 1995.

1. Goebel, S. J. *et al. Virology* **179,** 247–266 (1990).
2. Moss, B. in *Virology* (eds Fields, B. N. *et al.*) 2079–2111 (Raven, New York, 1990).
3. Payne, L. G. *J. gen. Virol.* **50,** 89–100 (1980).
4. Schmelz, M. *et al. J. Virol.* **68,** 130–147 (1994).
5. Morgan, C. *Virology* **73,** 43–58 (1976).
6. Stokes, G. V. *J. Virol.* **18,** 636–643 (1976).
7. Hiller, G., Weber, K., Schneider, L., Parajsz, C. & Jungwirth, C. *Virology* **98,** 142–153 (1979).
8. Hiller, G. & Weber, K. *J. Virol.* **44,** 647–657 (1982).
9. Hiller, G., Jungwirth, C. & Weber, K. *Expl Cell Res.* **132,** 81–87 (1981).
10. Krempien, U. *et al. Virology* **113,** 556–564 (1981).
11. Pollard, T. D. *Curr. Biol.* **5,** 837–840 (1995).
12. Cossart, P. *Curr. Opin. Cell Biol.* **7,** 94–101 (1995).
13. Tilney, L. G. & Portnoy, D. A. *J. Cell Biol.* **109,** 1597–1608 (1989).
14. Heinzen, R. A., Hayes, S. F., Peacock, M. G. & Hackstead, T. *Infect. Immun.* **61,** 1926–1935 (1993).
15. Bernardini, M. L., Mounier, J., d'Hauteville, H., Coquis-Rondon, M. & Sansonetti, P. J. *Proc. natn. Acad. Sci. U.S.A.* **86,** 3867–3871 (1989).
16. Blasco, R. & Moss, B. *J. Virol.* **66,** 4170–4179 (1992).
17. Hiller, G., Eibl, H. & Weber, K. *J. Virol.* **39,** 903–913 (1981).
18. Kato, N., Eggers, H. J. & Rolly, H. *J. exp. Med.* **129,** 795–808 (1969).
19. Payne, L. G. & Kristenson, K. *J. Virol.* **32,** 614–622 (1979).
20. Schmutz, C., Payne, L. G., Gubser, J. & Wittek, R. *J. Virol.* **65,** 3435–3442 (1991).
21. Dabiri, G. A., Sanger, J. M., Portnoy, D. A. & Southwick, F. S. *Proc. natn. Acad. Sci. U.S.A.* **87,** 6068–6072 (1990).
22. Theriot, J. A., Mitchison, T. J., Tilney, L. G. & Portnoy, D. A. *Nature* **357,** 257–260 (1992).
23. Payne, L. G. & Kristensson, K. *Archs Virol.* **74,** 11–20 (1982).
24. Kocks, C. *et al. Cell* **68,** 521–531 (1992).
25. Gouin, E., Dehoux, P., Mengaud, J., Kocks, C. & Cossart, P. *Infect. Immun.* **63,** 2729–2737 (1995).
26. Domann, E. *et al. EMBO J.* **11,** 1981–1990 (1992).
27. Blasco, R., Cole, N. B. & Moss, B. *J. Virol.* **65,** 4598–4608 (1991).
28. Marchand, J.-B. *et al. J. Cell Biol.* **130,** 1–13 (1995).
29. Herzog, M., Draeger, A., Ehler, E. & Small, J. V. *Cell Biology: A Laboratory Handbook* (Academic, San Diego, 1994).
30. Rodriguez, J. F., Janeczko, R. & Esteban, M. *J. Virol.* **56,** 482–488 (1985).

ACKNOWLEDGEMENTS. We thank Y. Rivière, V. David and E. Gouin for help in preliminary experiments; R. Blasco for vRB 12 and profilin null virus; D. Klaus and M. Esteban for the S1 myosin and C3 antibody, respectively; C. Dotti for help and suggestions concerning video microscopy; I. Reckmann for vaccinia virus preparations; S. Schleich for help with electron microscopy; and A. Hyman, K. Simons, M. Zerial, R. Parton and E. Karsenti for suggestions and comments on the manuscript.

Microtubule nucleation by γ-tubulin-containing rings in the centrosome

Michelle Moritz, Michael B. Braunfeld*, John W. Sedat*, Bruce Alberts† & David A. Agard*

Department of Biochemistry & Biophysics and
* Howard Hughes Medical Institute, University of California at San Francisco, 513 Parnassus Avenue, San Francisco, California 94143-0448, USA

THE microtubule cytoskeleton of animal cells does not assemble spontaneously, but instead requires the centrosome. This organelle consists of a pair of centrioles surrounded by a complex collection of proteins known as the pericentriolar material (PCM)[1]. The PCM is required for microtubule nucleation[2]. The minus, or slow-growing, ends of microtubules are embedded in the PCM and the plus, or fast-growing, ends project outwards into the cytoplasm during interphase, or into the spindle apparatus during mitosis. γ-Tubulin is the only component of the PCM that is so far implicated in microtubule nucleation[3–6]. Here we use immuno-electron microscopic tomography to show that γ-tubulin is localized in ring structures in the PCM of purified centrosomes without microtubules. When these centrosomes are used to nucleate microtubule growth, γ-tubulin is localized at the minus ends of the microtubules. We conclude that microtubule-nucleating sites within the PCM are ring-shaped templates that contain multiple copies of γ-tubulin.

We previously reported that the PCM of isolated *Drosophila* centrosomes that lack microtubules (MTs) contains hundreds of ring-like structures that are 25–30 nm in diameter and 10–13 nm thick. In addition, we found that the minus ends of MTs in centrosomes with regrown asters appear to be blunt and arise abruptly, inasmuch as they are not associated with any discernible structure[7]. We suggested then that the ring structures are MT-nucleating sites. Because their diameter is similar to that of MTs, they could be invisible at the minus ends of MTs in centrosomes with regrown asters. If these suggestions are correct,

TABLE 1 Distribution of gold particles in PCM of centrosomes with and without microtubules

	Number of gold particles (% total particles)		
(*a*) Centrosomes with MTs	At (−) ends of MTs	Ambiguous position	Total
All gold	77 (65%)	41 (35%)	118 (100%)
Single gold particles	2 (2%)	7 (6%)	
Clusters of 2	12 (10%)	8 (7%)	
Clusters of 3	15 (13%)	12 (10%)	
Clusters of 4	24 (20%)	8 (7%)	
Clusters of >4	24 (20%)	6 (5%)	
(*b*) Centrosomes without MTs	At ring structures	Ambiguous position	Total
All gold	68 (69%)	30 (31%)	98 (100%)
Single gold particles	3 (3%)	6 (6%)	
Clusters of 2	12 (12%)	8 (8%)	
Clusters of 3	12 (12%)	3 (3%)	
Clusters of 4	36 (37%)	0 (0%)	
Clusters of >4	5 (5%)	13 (13%)	

The gold particles were randomly chosen in each reconstruction and their association with identifiable structures (MTs or rings) was then determined by stepping through the relevant projections from the reconstruction, which reveals the three-dimensional structure of objects.

† Present address: National Academy of Sciences, 2101 Constitution Avenue NW, Washington, DC 20418, USA.

© 1995 Nature Publishing Group